Physica D 35 (1989) 237–250
North-Holland, Amsterdam

QUANTIFYING LOCAL PREDICTABILITY IN PHASE SPACE

Jon M. NESE
Department of Meteorology, The Pennsylvania State University, University Park, PA 16802, USA

Received 20 November 1987
Revised manuscript received 11 October 1988
Communicated by R.M. Westervelt

Both the classical Lyapunov exponents and the quantities from which they are derived, the local divergence rates, characterize the behavior of initially adjacent trajectories in phase space. The exponents are the long-term averages of this divergence, while the local rates quantify the behavior of nearby trajectories as a function of time and phase space position. Thus, given a transient-free initial state, the local divergence rates provide estimates of short-term predictability along the resultant trajectory. We calculate local divergence rates for the chaotic attractor of the three-component Lorenz model, and we investigate both the temporal and phase-spatial variations in predictability. We show quantitatively that predictability varies considerably with time, but that there is phase-spatial organization to the variability. This underlying structure permits identification of regions in phase space of high and low predictability and, in some cases, it permits an estimate of predictability to be assigned to the predictability variable itself.

1. Introduction

Lyapunov exponents measure the long-term average exponential rate of divergence or convergence of initially adjacent phase space trajectories on an attractor, and thus quantify average predictability properties. When at least one Lyapunov exponent is positive, the attractor is chaotic and initially nearby trajectories diverge exponentially, on average. For these attractors, the largest Lyapunov exponent defines a predictability time scale – the average time beyond which deterministic predictions become meaningless owing to the propagation of initial errors over the entire attractor. An increase in the magnitude of the largest Lyapunov exponent implies a decrease in the predictability time scale.

In general, nearby trajectories need not diverge at the same rate on all parts of a chaotic attractor. This idea has been quantified in various ways. Grassberger and Procaccia [17] model the fluctuations in the local divergence rate using methods from probability theory. Farmer and Sidorowich [18] present a technique for short-term forecasting of chaotic data that utilizes local phase space information. Nicolis et al. [1] propose calculating a "non-uniformity factor", which is defined as the variance of the local divergence rate. They calculate this factor for several model systems, including the Hénon and Rossler attractors. Dutton and Wells [2] have shown qualitatively for the Lorenz attractor [3] that adjacent trajectories converge in some parts of the phase space, even though these trajectories will separate eventually. This variability of the local divergence rate in phase space can result from the proximity of trajectories to unstable fixed points and their stable and unstable manifolds. Dutton and Wells [2] and Shirer [4] suggested this relationship in their characterization of unstable points as "decision points". This phase-spatial inhomogeneity in the local divergence rate of nearby trajectories is equivalent to a phase-spatial variability in the predictability time scale. Clearly, if predictability on a chaotic attrac-

tor is a function of time (and thus of phase space position), and if short time scales are of interest, then the local divergence rates are more relevant empirical measures of predictability than the classical Lyapunov exponents. In such cases, an understanding of the temporal and phase-spatial variations in the local divergence rate is necessary for a complete quantification of the predictability of the system.

Atmospheric science is one discipline particularly concerned with predictability on short time scales. Although rigorous proof that a finite-dimensional attractor exists for the full equations of atmospheric motion is lacking, theoretical progress has been made recently towards this end [5–7]. In addition, the dimensionality and predictability of attractors reconstructed from time series of observed weather variables have been estimated empirically [13,14], yielding small fractal dimensions between three and six and predictability time scales on the order of two weeks. If such a finite-dimensional attractor for atmospheric flows exists, then the irregular, aperiodic, and notoriously unpredictable nature of the weather would suggest that this attractor is likely to be chaotic, and likely to possess the property of non-uniformity of predictability time scale in phase space. Roads [8] and Tennekes et al. [9], among others, propose that on such an attractor predictability itself might have to be treated as a forecast variable. Legras and Ghil [15] and Nese [16] have demonstrated that temporal variations of the local divergence rate occur in phase space for chaotic attractors in atmospheric general circulation models of intermediate size.

We use the classic Lorenz attractor [3,12] as an example to investigate quantitatively both the temporal and phase-spatial variability of predictability on a chaotic attractor. First, we calculate the non-uniformity factor and summarize the temporal variability of the largest local divergence rate. Then, we show that on this attractor the local divergence rate exhibits an interesting phase-spatial organization. This organization can be used to identify regions on the attractor where adjacent trajectories converge or diverge and thus predictability is high or low, and also to identify regions where the sign of the local divergence rate is itself predictable or unpredictable. This phase-spatial structure is demonstrated in two ways: first, by constructing several Poincaré sections of the attractor, and second, by isolating various regions of the phase space and averaging the largest local divergence rate at points on the attractor in those regions.

2. Methodology

Given an N-dimensional dynamical system of ordinary differential equations

$$\dot{x}_i(t) = F_i(x_1(t),\ldots,x_N(t)), \quad i = 1,2,\ldots,N, \tag{1}$$

the largest Lyapunov exponent can be defined [1, 10] as

$$\lambda_1 = \lim_{t\to\infty} \frac{1}{t} \log_2 \frac{\|z(t)\|}{\|z(0)\|}, \tag{2}$$

where $z(t) = (z_1(t),\ldots,z_N(t))$ is an infinitesimal perturbation of the trajectory $x(t) = (x_1(t), \ldots,x_N(t))$. The perturbation $z(t)$ evolves in the tangent space to $x(t)$ according to the linearized equations

$$\dot{z}_i(t) = \frac{\partial F_i}{\partial x_j} z_j(t), \quad i,j = 1,\ldots,N. \tag{3}$$

In practice, $z(t)$ is renormalized frequently while computing λ_1. If time is written as $t = k\tau$, $k = 0,1,2,\ldots$, then a local divergence rate $L(x(k\tau))$ can be defined as

$$L(x(k\tau)) = \frac{1}{\tau} \log_2 \frac{\|z((k+1)\tau)\|}{\|z(k\tau)\|}, \quad k = 0,1,\ldots \tag{4}$$

where it is easily shown that

$$\lambda_1 = \lim_{n\to\infty} \frac{1}{n} \sum_{k=0}^{n} \left[\frac{1}{\tau} \log_2 \frac{\|z((k+1)\tau)\|}{\|z(k\tau)\|} \right]$$

$$= \lim_{n\to\infty} \frac{1}{n} \sum_{k=0}^{n} L(x(k\tau)). \tag{5}$$

That is, the time average of the local divergence rate, as $t \to \infty$, is the largest Lyapunov exponent. The non-uniformity factor ΔL is then defined by

$$(\Delta L)^2 = \lim_{n\to\infty} \frac{1}{n} \left[\sum_{k=0}^{n} [L(x(k\tau))]^2 \right] - \lambda_1^2, \tag{6}$$

which measures the variability of the local divergence rate over the attractor [1].

For a chaotic attractor, the largest Lyapunov exponent λ_1 defines a predictability time scale by quantifying the average rate at which initial uncertainty is propagated over the attractor. The Lyapunov exponents are typically expressed in units of bits of information per unit time. For example, if the initial conditions are known to be accurate to q bits, then after approximately q/λ_1 units of time, on average, the initial uncertainty will have contaminated the entire attractor.

The Lorenz system [3] consists of three nonlinear ordinary differential equations representing the phase space evolution of certain Fourier coefficients X, Y, and Z of Rayleigh–Bénard convection. The dimensionless system is given by

$$\dot{X} = PY - PX, \tag{7}$$

$$\dot{Y} = RX - Y - XZ, \tag{8}$$

$$\dot{Z} = XY - bZ, \tag{9}$$

in which the Rayleigh number R, the forcing parameter, is proportional to the imposed vertical temperature gradient, b is related to the aspect ratio of the domain, and P is the Prandtl number of the fluid. For $R = 28$, $b = 8/3$, and $P = 10$, Lorenz's original parameter choices, the system has three fixed points, all unstable, at the origin and at $(\pm\sqrt{72}, \pm\sqrt{72}, 27)$. A transient-free solution trajectory generated by integrating (7)–(9) is shown in fig. 1; dots mark the locations of the three fixed points. Empirically, the attractor is chaotic and has classical Lyapunov exponents 1.3, 0.0, and −21.1 bits per dimensionless time unit (bpt).

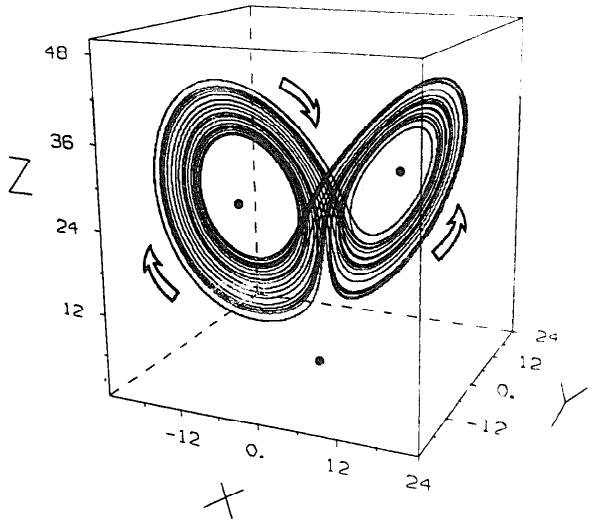

Fig. 1. A computer-generated solution trajectory for the Lorenz system, for parameter values $R = 28$, $b = 8/3$, and $P = 10$. The arrows indicate the direction of the flow, and dots mark the locations of the three unstable fixed points.

Our study consists of two parts. First, we investigate only the temporal variation of the local divergence rate of adjacent trajectories on the Lorenz attractor, ignoring for the moment the dependence on phase space position. We calculate the non-uniformity factor of the attractor and the probability distribution of the local divergence rate. Second, we demonstrate that there is underlying organization in the phase-spatial variation of the local divergence rate. To accomplish this, we construct several Poincaré sections and show that on some parts of the attractor it is possible to predict short-term error growth, even if the phase

space location is known only approximately. Then, to yield a more global picture of how predictability varies on the attractor, we somewhat arbitrarily isolate various regions of the phase space that contain portions of the attractor, and compute the average of the local divergence rate over 5×10^5 points on the attractor in each of these regions. Because the Lorenz system possesses the inherent symmetry $(X, Y, Z) \rightarrow (-X, -Y, Z)$, we consider only one wing of the attractor in most of the analyses.

Our calculations are performed on a Cray X-MP/48 computer, which provides approximately 14 digits of accuracy. To integrate the equations, we use the IMSL subroutine DVERK, a Runge-Kutta 5th- and 6th-order method, with stepsize $\tau = 2 \times 10^{-3}$. Numerical tests with (7)–(9) confirm that this routine exhibits the expected 5th- and 6th-order convergence. In all experiments, the first 2×10^4 iterations are discarded to ensure transient-free behavior. The mean orbital period (the average time required for one circuit around a wing of the attractor) is slightly less than one dimensionless time unit, so this number of iterations corresponds to approximately 40 circuits.

3. Temporal variation of predictability

Fig. 2 shows the variation of the local divergence rate as a function of dimensionless time $t = k\tau$ for a portion of a typical trajectory on the attractor. Two different units for $L(\boldsymbol{x}(t))$ are shown. The first is bits per dimensionless time unit (bpt), which derives directly from the definition of local divergence rate. The second is an "instantaneous" e-folding time (cast now in dimensional units); this is the approximate value that the e-folding time would have if the instantaneous values of $L(\boldsymbol{x}(t))$ were constant over the entire attractor. Obviously, predictability varies widely over the attractor. Integrating for 2×10^6 time steps, we find a minimum value of $L(\boldsymbol{x}(t))$ of approximately -15 bpt, while the maximum value exceeds 16 bpt. Not surprisingly, the curve appears to be almost periodic at times; however, the variance spectrum of $L(\boldsymbol{x}(t))$ (not shown), like the spectra of X, Y, and Z, shows no distinct peaks at any frequency. The non-uniformity factor ΔL is correspondingly large, and is 6.1 bpt.

We can further characterize the temporal variations of predictability on a chaotic attractor by

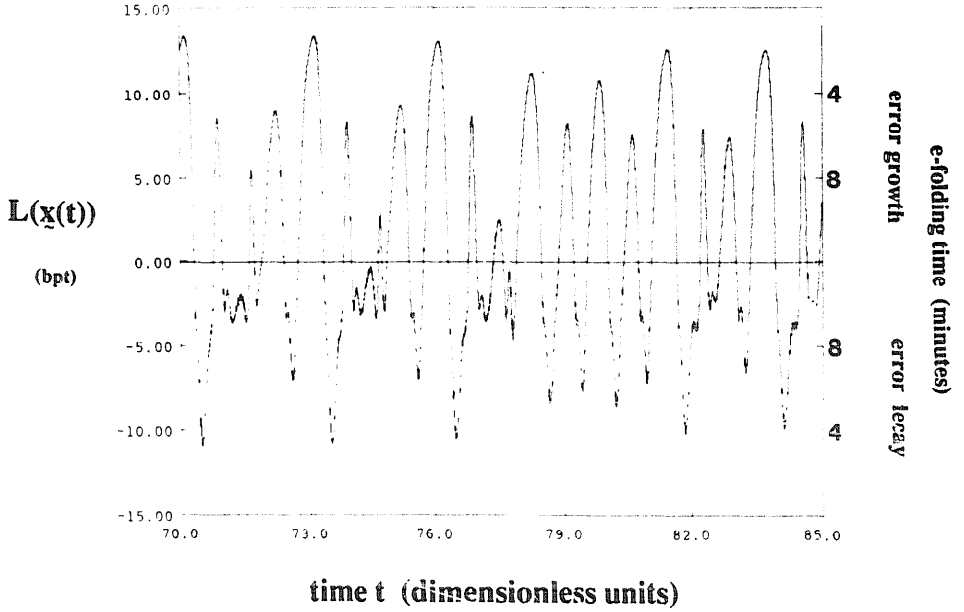

Fig. 2. The local divergence rate $L(\boldsymbol{x}(t))$ for the dimensionless time interval $70 \leq t \leq 85$.

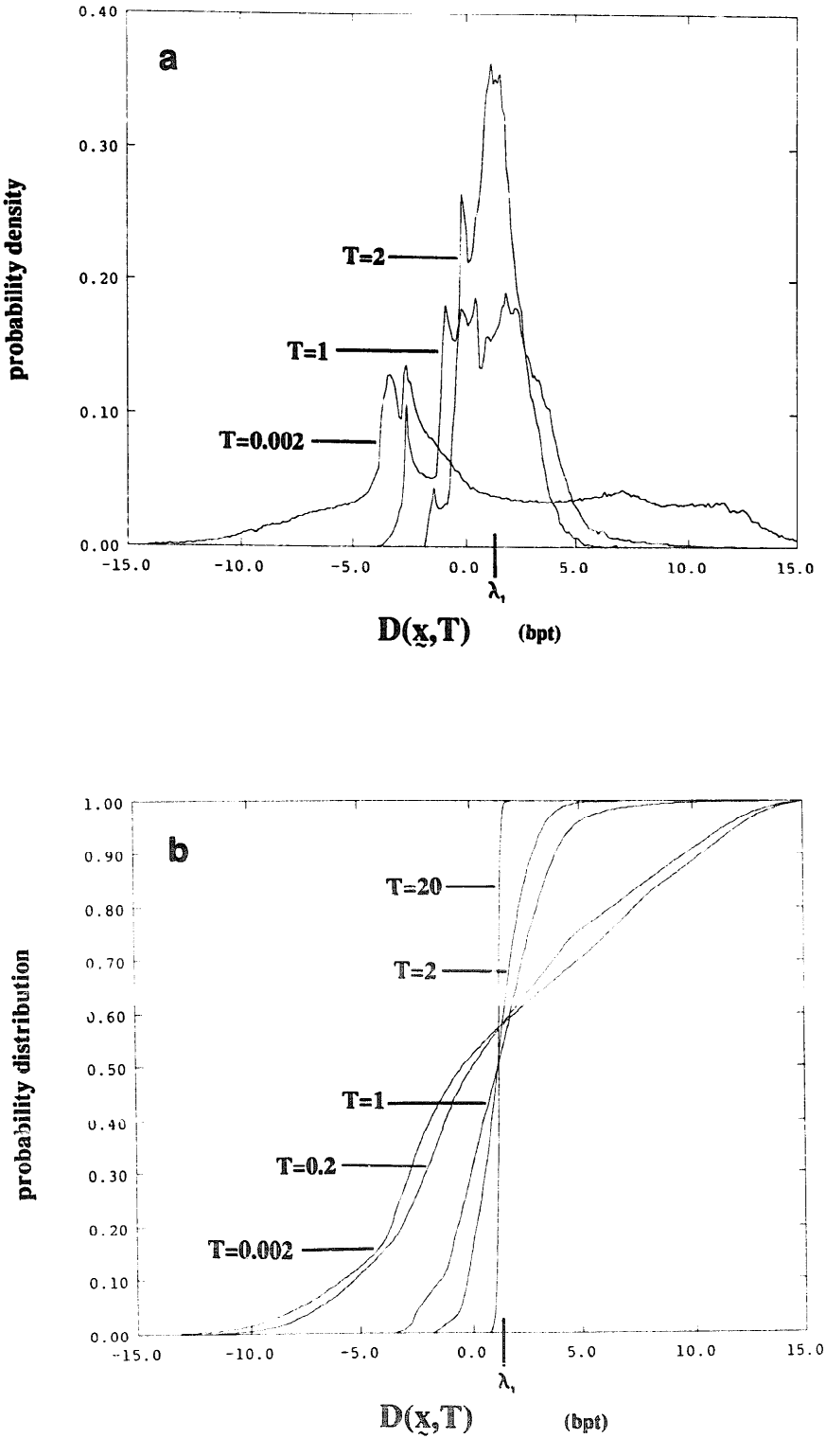

Fig. 3. (a) Estimated probability density curves for $D(x, T)$ for $T = 0.002$, $T = 1$, and $T = 2$. An interval $\Delta D(x, T) = 0.1$ bpt was used to construct the histograms that approximate these curves. (b) Integrals of the probability density curves of $D(x, T)$, for $T = 0.002$, 0.2, 1, 2, and 20.

calculating a function $D(x, T)$, where $D(x, T)$ is the time-average of the local divergence rate over the first j iterations of a trajectory emanating from a point x on the attractor, and $T = j\tau$, $j = 1, 2, \ldots$. For $j = 1$, $D(x, T) = D(x, \tau)$ is simply a local divergence rate, whereas $D(x, \infty)$ would yield the largest Lyapunov exponent (for almost all choices of points x). Calculating $D(x, T)$ for values of j, $1 < j < \infty$, gives information about predictability on intermediate time scales. We evaluate $D(x, T)$ for $T = 0.002$, 0.2, 1, 2, and 20 dimensionless time units (corresponding to $j = 1$, 100, 500, 1000, and 10000, respectively) at 1×10^6 randomly chosen points on the attractor.

Fig. 3(a) shows the probability density curves for three of these values of T, approximated by choosing an interval $\Delta D(x, T) = 0.1$ bpt. In addition, fig. 3(b) shows the probability distribution curves for all five values of T. The value of λ_1 is indicated on the abscissa in both figures. Interestingly, the peaks in the probability density curve for $T = 0.002$ occur at strongly negative values, -3.3 and -2.6 bpt. From fig. 3(b), we see that Prob $[D(x, 0.002) < 0] \approx 0.52$, and Prob $[D(x, 0.002) < \lambda_1] \approx 0.57$ in this case. Similarly, for $T = 0.2$ (not shown in fig. 3(a)), the peak in the probability density curve occurs for negative values of $D(x, 0.2)$, near -1.5 bpt, and Prob $[D(x, 0.2) < \lambda_1] \approx 0.57$ as well. Fig. 3(a) shows that even for $T = 1$, a time slightly greater than the mean orbital period, relative maxima occur at -2.6, -0.9, and -0.2 bpt, and Prob $[D(x, 1) < 0] \approx 0.30$. By $T = 2$, the peak near $D(x, 2) = \lambda_1$ is fairly well-established, but a secondary peak at $D(x, 2) \approx -0.2$ persists. From fig. 3(b), we find that Prob $[D(x, 2) < 0] \approx 0.15$, which is still a non-trivial value, especially considering that $T = 2$ is more than twice the mean orbital period. The smallest value of T for which Prob $[D(x, T) < 0] = 0$ is approximately $T = 9$. Fig. 3(b) shows that by $T = 20$, $D(x, 20)$ is always between 0.6 and 2.0 bpt.

Thus, a very different picture of predictability on the attractor emerges when various time scales are considered. The peak in the probability density curve, rather than being simply a quasi-stationary feature that changes only in amplitude with changing T, occurs at negative values of $D(x, T)$ for small enough T, and shifts toward λ_1 as T increases.

4. Phase-spatial variation of predictability

4.1. *Poincaré sections*

We begin our analysis of the phase-spatial structure of the local divergence rate by constructing several Poincaré sections of the attractor. The first map, constructed from 4×10^3 intersections of a trajectory with the plane $X = -9$, is shown in fig. 4(a). On the lower piece of the map, $\dot{X} < 0$, while $\dot{X} > 0$ for the upper piece. The pieces each appear to be continuous owing only to the finite resolution of the plotter. In fig. 4(b), for each point on the lower curve in fig. 4(a), we plot the local divergence rate as a function of the variable Z. For $Z < \approx 16$ and $Z > \approx 21.5$, the local divergence rate is always large and positive, indicating rapid growth of small perturbations. Although predictability is low owing to the large local divergence rates, this characteristic of the predictability is so phase-spatially consistent with varying Z that it is possible to predict not only that small errors will amplify, but also the approximate rate at which they will grow. In the intervening region $16 < Z < 21.5$, most points still have a positive local divergence rate, but the large scatter in the values indicates that the phase-spatial smoothness in $L(x(t))$ is absent, and so the ability to predict future error growth is greatly reduced.

Fig. 4(c) is the same as fig. 4(b), except for the upper curve in fig. 4(a). Here it is more convenient to plot the local divergence rate as a function of the variable Y. Again, a distinct organization of the local predictability is evident. Only for $Y < \approx -5$ can $L(x(t))$ be positive; for $Y > \approx -5$, all local divergence rates are negative. The local divergence rate decreases linearly, on average, with increasing Y. Thus, predictability is high on this part of the attractor not only because most adjacent trajecto-

ries converge, but also because there is a clear, predictable structure in the way by which predictability varies in the phase space.

We now consider a second Poincaré section. In fig. 5(a) we plot 8×10^3 points of intersection of a trajectory with the plane $Z = 26$. For the points on the lower left and upper right curves, $\dot{Z} > 0$, while $\dot{Z} < 0$ for the points on the two middle curves. In fig. 5(b), the local divergence rate associated with the points on the lower left curve is

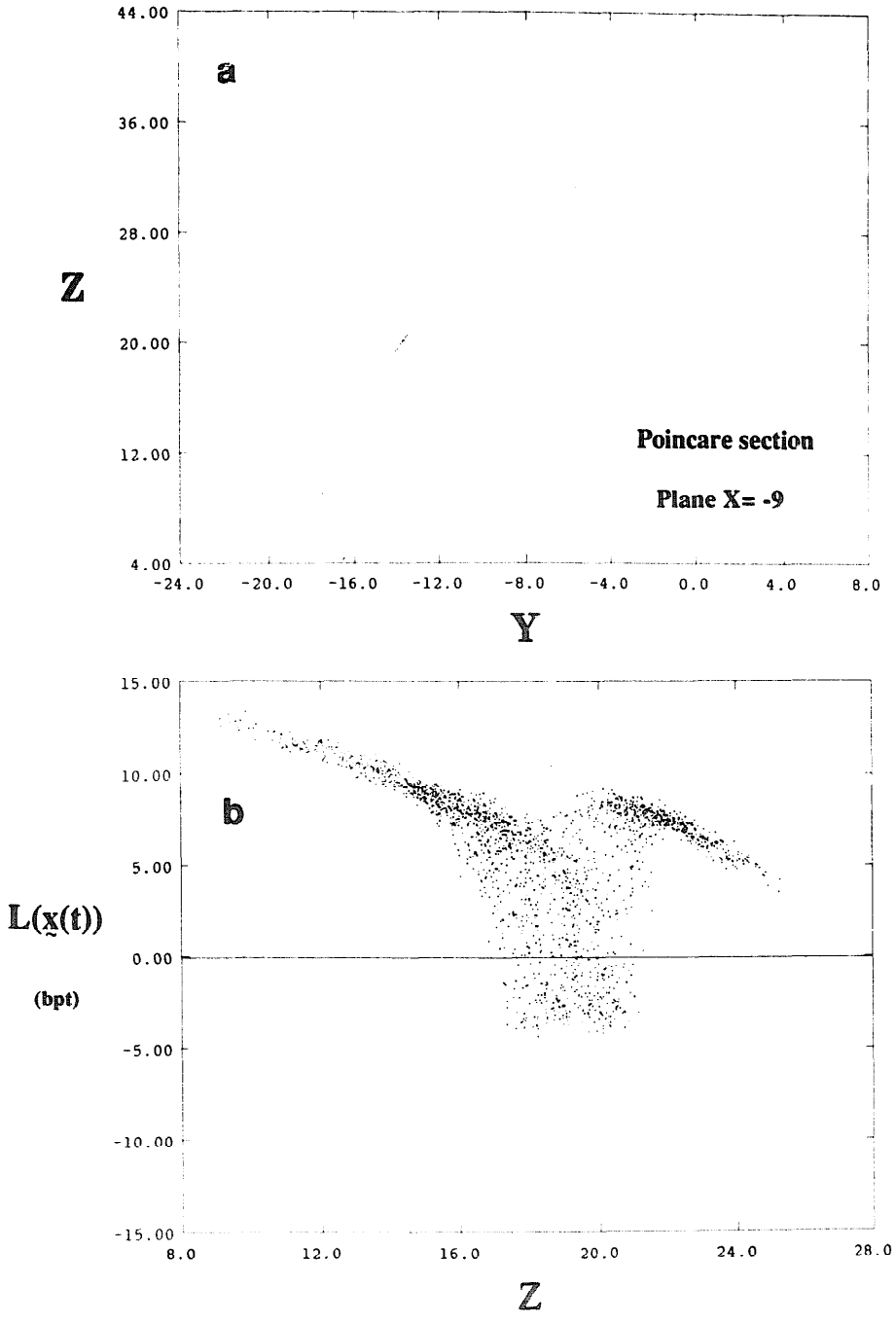

Fig. 4. (a) 4×10^3 points of intersection of a trajectory on the Lorenz attractor with the plane $X = -9$. (b) The value of the local divergence rate at each point on the lower curve in (a), plotted as a function of Z. (c) The value of the local divergence rate at each point on the upper curve in (a), plotted as a function of Y.

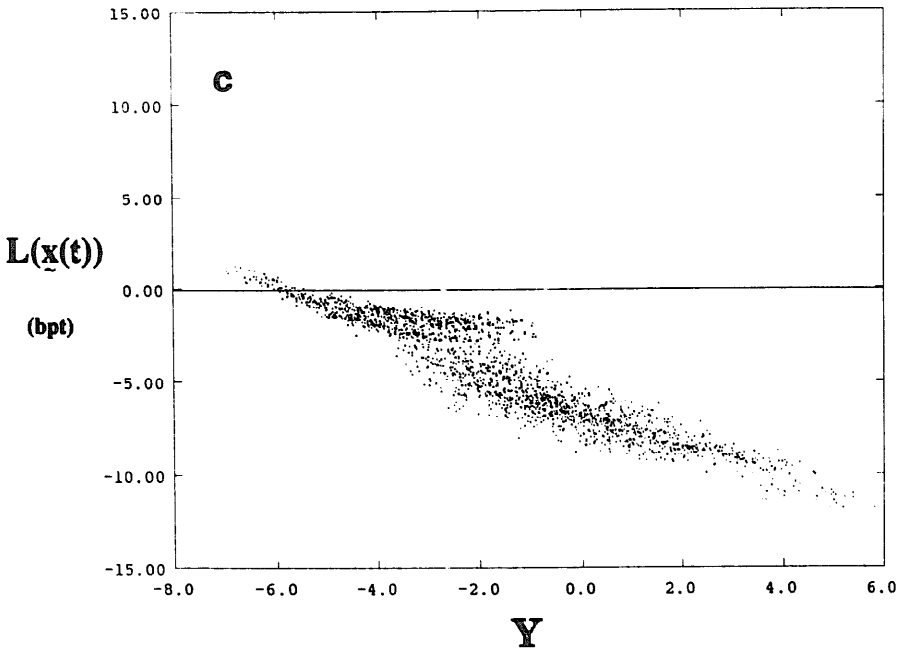

Fig. 4. Continued.

plotted as a function of X (fig. 5(b) also applies to the upper right curve in fig. 5(a), with X replaced by $-X$). Several distinct regimes of predictability are again apparent. For $X < \approx -13.5$ and for $X > \approx -11.5$, adjacent trajectories diverge, in most cases at a relatively slow rate. Again, although local predictability is low in the sense that small perturbations will amplify on short time scales, this property of predictability is itself highly predictable. The situation in the range $-13.5 < X < -11.5$ is more complicated; adjacent trajectories may diverge or converge, and there is a much more limited ability to know which will occur.

Finally, in fig. 5(c), we plot the local divergence rate for the points on the two middle curves in fig. 5(a), again as a function of X. We plot $L(x(t))$ for both curves to show the inherent symmetry. For $X < \approx -5$ and $X > \approx -1$ on the top curve and for $X > \approx 5$ and $X < \approx 1$ on the bottom curve, predictability is high not only because adjacent trajectories converge but also because the rate of local convergence varies in a reasonably predictable manner with changes in X. Again, predictability in the intervening ranges of X on both curves is less consistent, both in terms of the magnitude of the divergence or convergence and in the ability to predict the type of behavior.

4.2. *Averaging over portions of trajectories*

We now attempt a more general description of the phase-spatial variability of predictability by considering averages of the local divergence rates on various regions of the attractor. We compute the average of $L(x(t))$ for nine volumes that contain portions of the attractor; in each volume, 5×10^5 points on the attractor are used. For convenience, we choose to bound these regions of phase space using planes of the form X = constant and Z = constant, thereby ignoring variations in the Y-direction. The volumes are shown in figs. 6(a)–(i). The averages of the local divergence rates for the nine regions shown in figs. 6(a)–(i) appear in table I, as do the standard deviations of the averages.

In experiments (a)–(d) we consider trajectories in the vicinity of the Z-axis and the origin, a region whose dynamics is strongly controlled by the unstable fixed point at (0,0,0) and by its two-dimensional stable and one-dimensional un-

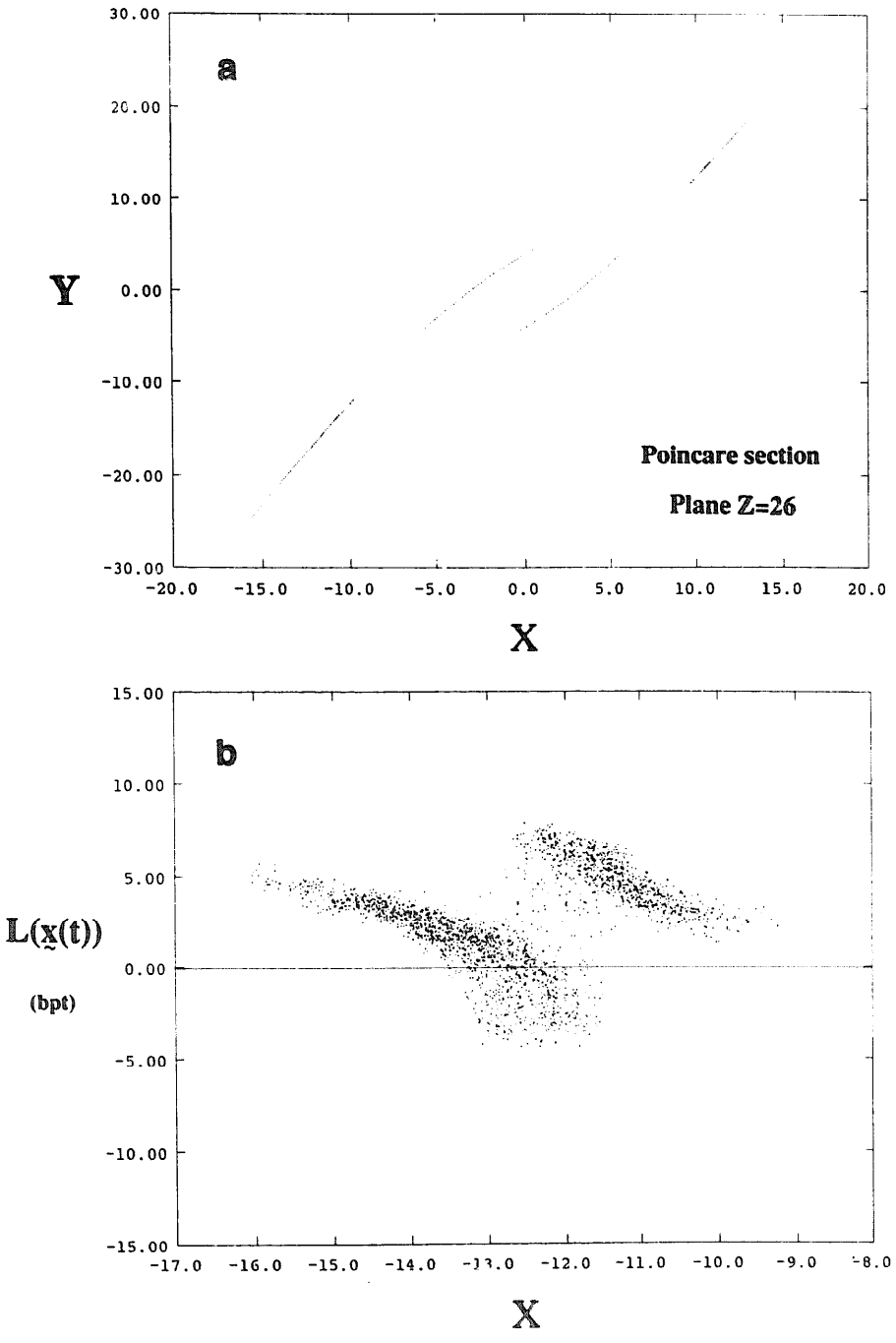

Fig. 5. (a) 8×10^3 points of intersection of a trajectory on the Lorenz attractor with the plane $Z = 26$. (b) The value of the local divergence rate at each point on the lower curve in (a), plotted as a function of X. (c) Same as in (b), except for the two middle curves.

stable manifolds. Significantly, the stable manifold of the origin contains the Z-axis. The origin is the crucial decision point in the phase space of the Lorenz system [2, 4, 11]; trajectories swinging toward it must "decide" which of the two wings of the attractor to visit next. More precisely, this part of the attractor is the major source of long-term errors because the potential exists for nearby trajectories to separate rapidly each time a circuit is completed around a wing of the attractor.

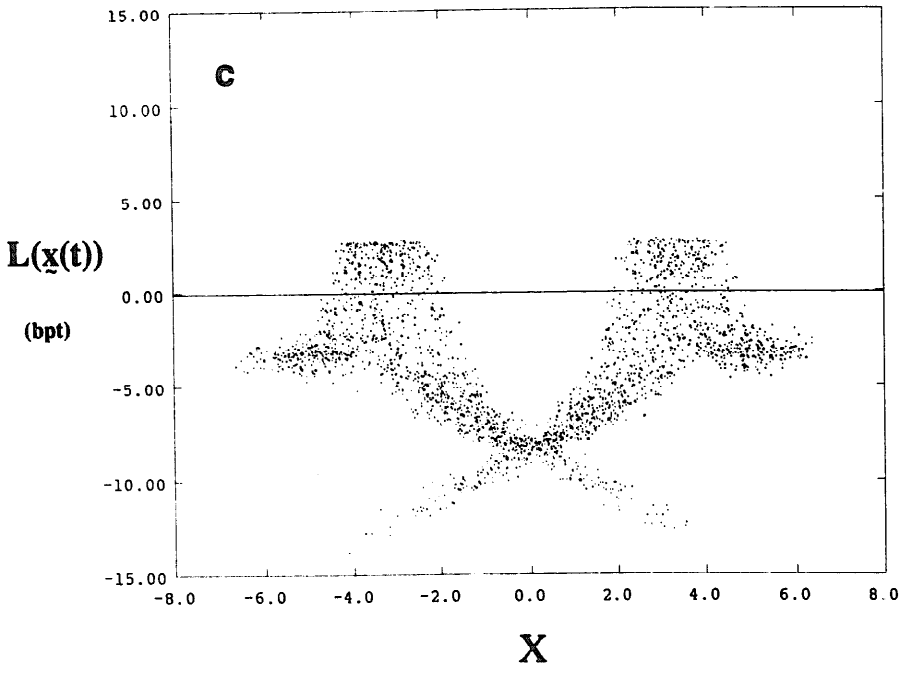

Fig. 5. Continued.

The short-term description of this region is somewhat different, however. The results of experiments (a), (b), and (c), as well as figs. 4(c) and 5(c), show that trajectories nearing the Z-axis and approaching the origin from above (and thus nearing the stable manifold of the origin) converge, on average, when far enough from the unstable point. The average local divergence rate is a minimum (-5.6 bpt) in region (a), and the standard deviation (3.6 bpt) indicates that almost all pairs of adjacent trajectories are converging in this region. Points in regions (a), (b), and (c) are prime contributors to the peaks at negative values of $D(x, T)$ in the probability density curves for $T = 0.002$, $T = 0.2$, and $T = 1$ that were discussed earlier.

Once trajectories enter the region of experiment (d), the potential exists for catastrophic separation and thus large amplitude errors, with one trajectory circling each wing. The ensemble average is correspondingly positive (3.8 bpt) and about three times as large as the long-term rate of divergence averaged over the entire attractor as measured by the largest Lyapunov exponent. Despite the potential for large amplitude errors, the average of $L(x(t))$ is not a maximum in this region; rather, adjacent trajectories diverge most rapidly on average low on the wing of the attractor in the regions of experiments (e) and (f), where trajectories are departing from the neighborhood of the origin. The strong divergence of adjacent trajectories near the plane $X = -9$ has already been illustrated in fig. 4(b). The errors that occur in these regions, however, are in the phase, or timing, of the solution, rather than the amplitude. Although the average local divergence rate is larger in regions (e)–(f), these phase errors produce, in general, less severe forecast problems than the large amplitude errors that can occur in region (d) when two initially nearby trajectories separate and circle different wings. These observations imply that the average divergence rates alone fail to distinguish this critical difference in the type and severity of the phase space errors. To this end, the standard deviations add crucial information; the pronounced maximum (6.2 bpt) in the standard deviation for region (d) reflects the extreme variability

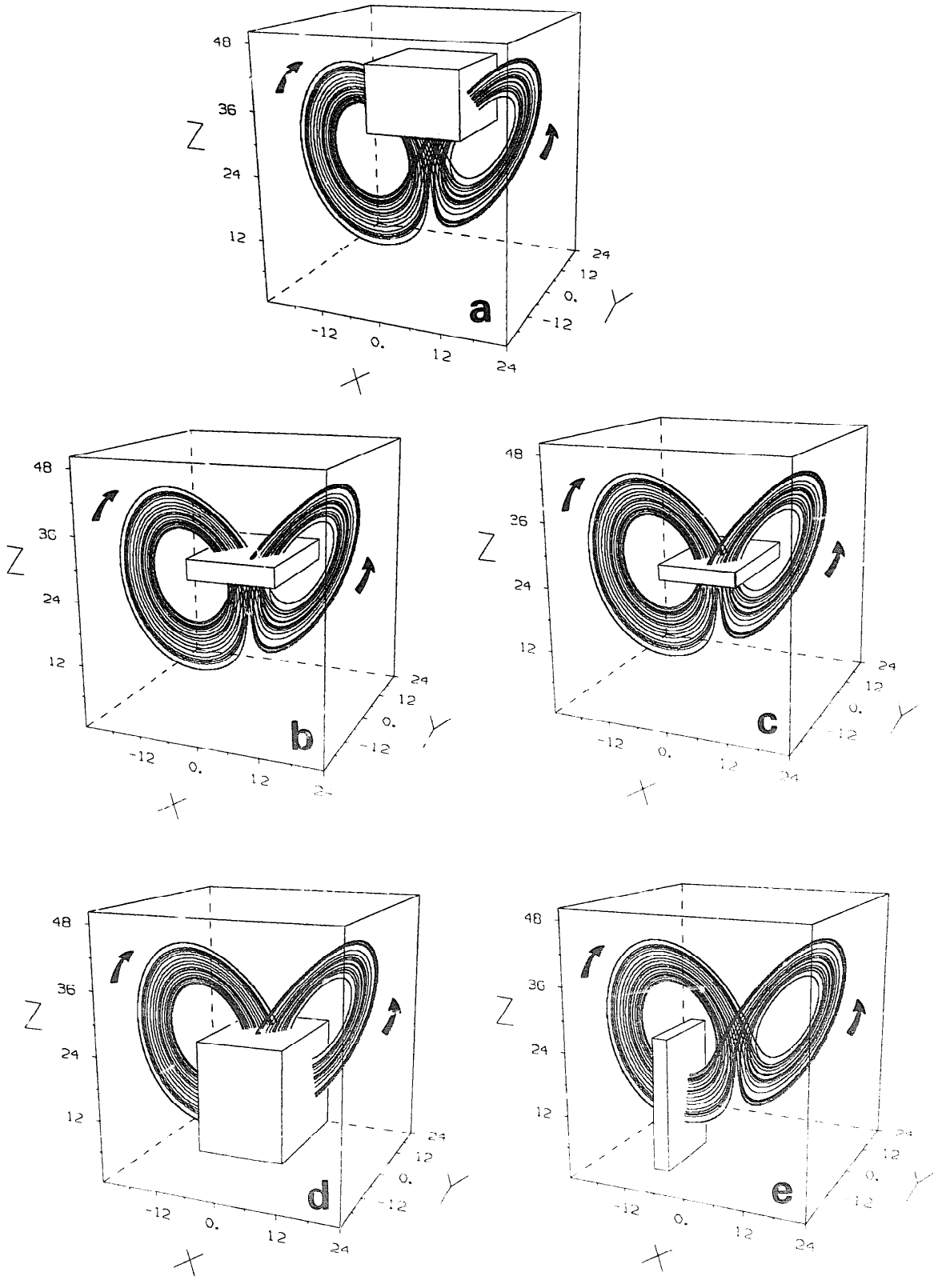

Fig. 6. The nine phase space regions for which we calculate the average of the largest local divergence rate. The volumes are classified according to the planes through which trajectories enter and exit. (a) Enter either $X = -9$ or $X = 9$, exit $Z = 30$. (b) Enter $Z = 30$, exit $Z = 26$. (c) Enter $Z = 26$, exit $Z = 23$. (d) Enter $Z = 26$, exit either $X = -6$ or $X = 6$. (e) Enter $X = -6$, exit $X = -9$. (f) Enter $X = -6$, exit $Z = 23$. (g) Enter $Z = 23$, exit $Z = 30$. (h) Enter $Z = 30$, exit $X = -9$. (i) Enter $X = -9$, exit $X = -6$.

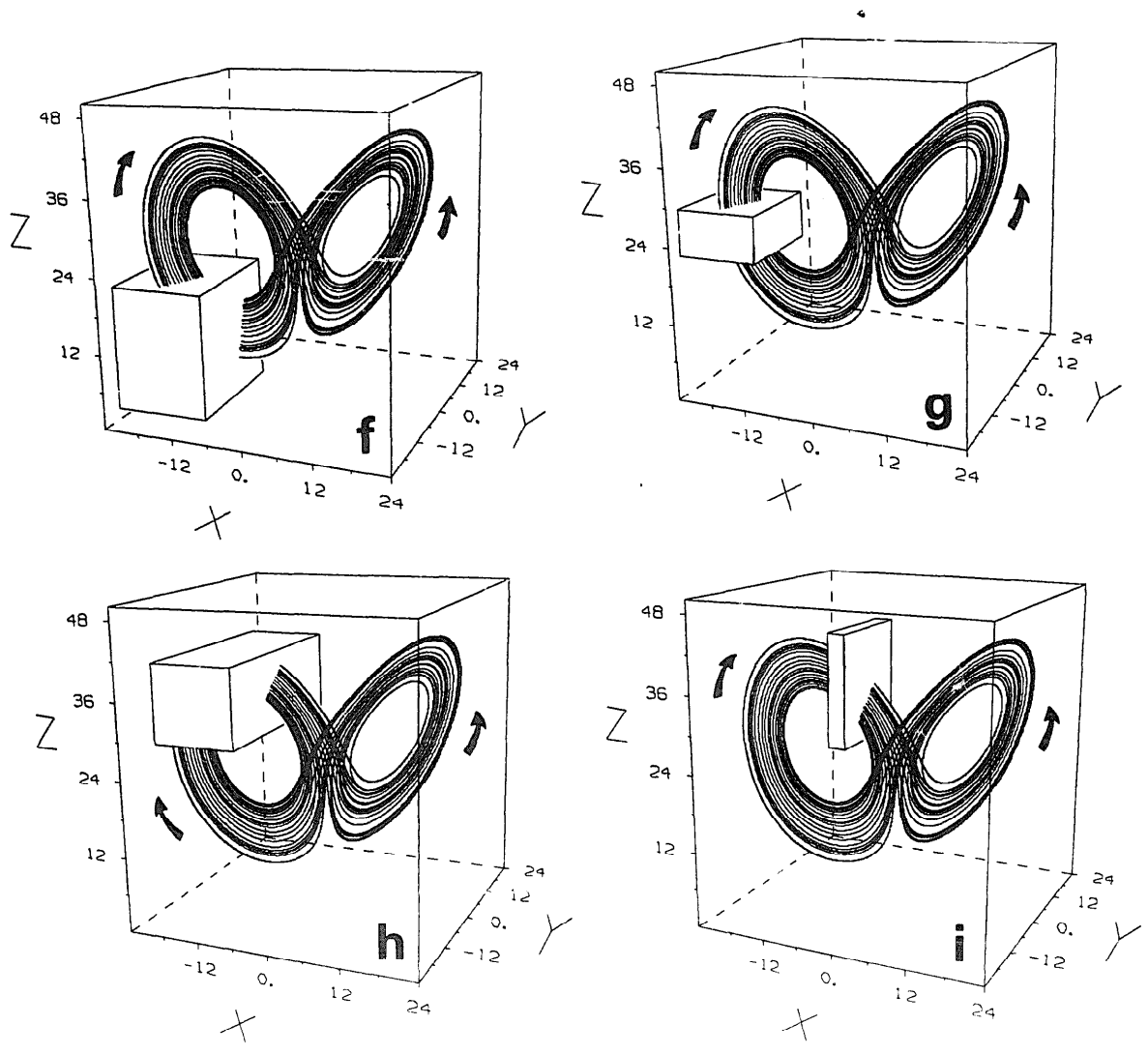

Fig. 6. Continued.

in the behavior of nearby trajectories in this volume, at least suggesting that trajectories are near a decision point in the phase space.

Continuing clockwise around the left wing of the attractor in experiments (g)–(i), we find that the average divergence rate decreases gradually, reaching zero in the vicinity of the plane $Z = 30$. The small magnitude of the ratio between the average divergence rate and its standard deviation for region (g) suggests that a transition from average divergence to average convergence occurs in this region. In the region of experiment (h), the average convergence rate is of order -3 bpt and the standard deviation is a minimum. By the time trajectories exit region (h) through the plane $X = -9$, nearly all pairs of adjacent trajectories converge, as we showed in fig. 4(c). This tendency for predictable short-term behavior persists as trajectories continue to approach the Z-axis through regions (i), (a), and (b).

5. Summary and concluding remarks

Traditionally in the analysis of a chaotic dynamical system, the Lyapunov exponents are calculated to quantify the notion of (un)predictability. The largest Lyapunov exponent defines the

Table I
The average of the largest local divergence rate and its standard deviation for the nine phase space volumes shown in figs. 6(a)–(i). For each volume, 5×10^5 points were considered.

Phase space volume	Average divergence rate (bpt)	σ (bpt)
a	−5.6	3.6
b	−4.3	3.6
c	−2.9	3.4
d	3.8	6.2
e	5.2	4.4
f	5.4	4.2
g	1.3	4.4
h	−2.7	2.2
i	−4.0	3.0

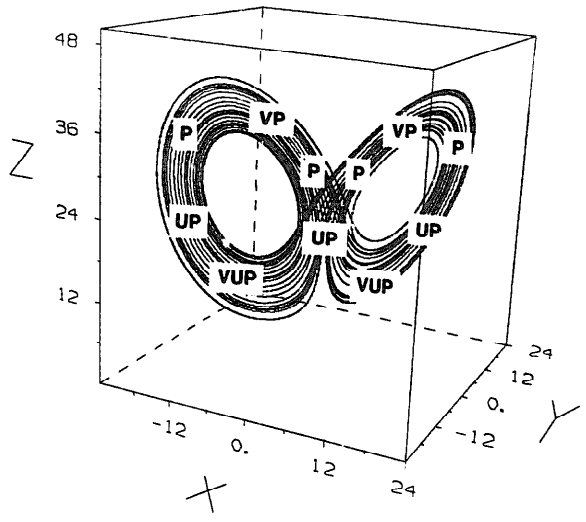

Fig. 7. Qualitative description of local predictability on the Lorenz attractor. The abbreviations VP, P, UP, and VUP denote very predictable, predictable, unpredictable, and very unpredictable regions, respectively.

predictability time scale of the system. However, the rate at which adjacent trajectories diverge on a chaotic attractor is, in general, not constant, but rather this local divergence rate depends on time and therefore, on location in phase space. Thus, for applications requiring short-term prediction, using only the classical Lyapunov exponents to measure predictability is inadequate because any phase-spatially dependent predictability information is essentially eliminated by averaging over the attractor. We study the local predictability of the three-variable Lorenz system from both temporal and phase-spatial viewpoints to demonstrate how the local divergence rates might be used to identify regions of high or low predictability in phase space.

Although the Lorenz attractor (for $R = 28$) is chaotic with largest Lyapunov exponent 1.3 bpt, the local divergence rate varies from −15 bpt to 16 bpt and the peaks in the probability density curve of $L(x(t))$ occur at negative values. Even when pairs of adjacent trajectories are followed for a time equal to one-fifth of the mean orbital period, approximately fifty percent of the pairs do not diverge. Thus, regardless of their asymptotic behavior, adjacent trajectories on parts of the attractor converge temporarily, some at very large rates. For example, once a trajectory swings back toward the Z-axis on either wing, its future, at least for short times, can in most cases be determined very accurately (in agreement with [2] and [11]). The local predictability of the Lorenz attractor is summarized qualitatively in fig. 7. We find that initially nearby trajectories converge most rapidly on average as they approach the vicinity of the Z-axis on the tops of the wings. Adjacent trajectories diverge most rapidly on average on the bottoms of the wings of the attractor as trajectories swing away from the vincinity of the unstable origin. However, our detailed analysis using Poincaré sections shows that even on a portion of the attractor where predictability is low owing to rapid divergence of nearby trajectories, there still may be a sense of predictability because the divergence may be a uniform characteristic of that region of the phase space. In these cases, the short-term error growth can be estimated.

Predictability near the Z-axis and origin is influenced by two opposing effects. For relatively large values of Z, almost all pairs of adjacent trajectories converge temporarily owing to the stabilizing influence of the Z-axis, which is part of the two-dimensional stable manifold of the origin. Closer to (0, 0, 0), the positive average reflects the potential that exists for extremely rapid divergence of neighboring trajectories, with one trajec-

tory circling each wing. However, this potential is only occasionally realized, as indicated by the maximum in the standard deviation of the average divergence rate. Thus the region near the origin, which is the principal source of long-term errors, is only moderately unpredictable in terms of average local divergence rates. Nonetheless, when catastrophic separation occurs, the consequences in terms of forecast errors are extremely severe.

We have used standard statistical analysis techniques, Poincaré maps, and phase-spatial averaging to quantify local predictability. Of course, such a study of local predictability could have been undertaken in many other ways. Regardless of the particular methods used, an analysis of both the temporal and phase-spatial variations of the local divergence rate is essential to a complete quantitative description of the predictability of a dynamical system. For a low-dimensional system such as the one studied here, such an analysis is both geometrically and computationally feasible. In higher-dimensional phase spaces, the temporal variation of predictability remains simple to compute, but identifying phase-spatial order in the local divergence rates becomes increasingly more difficult. Indeed, such order may not exist at all. Locating some of the unstable fixed points and their stable and unstable manifolds in such higher-dimensional phase spaces appears to be a reasonable first step in discovering any phase-spatial organization in local predictability.

Acknowledgements

I am indebted to Professors John A. Dutton, Hampton N. Shirer, Robert Wells, and Jerry L. Bona for their insightful comments and suggestions. The recommendations of an anonymous reviewer were extremely helpful as well. Most of the calculations reported in this paper were performed on the CRAY X-MP/48 at the Pittsburgh Supercomputing Center, which is funded by the National Science Foundation. I am particularly grateful to Joel Welling at PSC for his assistance with the three-dimensional graphics. This research was supported by the National Science Foundation through an NSF Graduate Fellowship and by the Earth Systems Science Center at Penn State University.

References

[1] J. Nicolis, G. Meyer-Kress and G. Haubs, Z. Naturforsch. 38a (1983) 1157.
[2] J.A. Dutton and R. Wells, in: Predictability of Fluid Motions, G. Holloway and B.J. West, eds. (Am. Inst. of Physics, New York, 1984), p. 11.
[3] E.N. Lorenz, J. Atmos. Sci. 20 (1963) 130.
[4] H.N. Shirer, in: Predictability of Fluid Motions, G. Holloway and B.J. West, eds. (Am. Inst. of Physics, New York, 1984), p. 355.
[5] R. Temam, Navier–Stokes equations and nonlinear functional analysis, CBMS/NSF Regional Conference Series in Applied Mathematics, 41, (Soc. of Industrial and Applied Mathematics, Philadelphia, 1983).
[6] C. Foias, G. Sell and R. Temam, Inertial manifolds for nonlinear evolutionary equations, Univ. of Minnesota, Inst. of Mathematical Applications, preprint 234 (March 1986).
[7] R. Wells and J.A. Dutton, Bull. Australian Math. Soc. 34 (1986) 321.
[8] J.O. Roads, J. Atmos. Sci. 42 (1985) 884.
[9] H. Tennekes, A.P.M. Baede and J.D. Opsteegh, Forecasting forecast skill, Internal memorandum DM-86-5. Royal Netherlands Meteorological Inst. (March 1986).
[10] A. Wolf, J. Swift, H. Swinney and J. Vastano, Physica D 16 (1985) 285.
[11] J.M. Nese, in: Nonlinear Hydrodynamic Modeling: A Mathematical Introduction, H.N. Shirer, ed. (Springer, New York, 1987), p. 384.
[12] C. Sparrow, The Lorenz Equations: Bifurcations, Chaos, and Strange Attractors (Springer, New York, 1982), 269 pp.
[13] K. Fraedrich, J. Atmos. Sci. 43 (1986) 419; 44 (1987) 722.
[14] H. Henderson and R. Wells, Adv. Geophys. 30 (1988) 205.
[15] B. Legras and M. Ghil, J. Atmos. Sci. 42 (1985) 433.
[16] J.M. Nese, PhD dissertation, Pennsylvania State Univ. (1989).
[17] P. Grassberger and I. Procaccia, Physica D 13 (1984) 34.
[18] J.D. Farmer and J.J. Sidorowich, Phys. Rev. Lett. 59 (1987) 845.